Improved beam characteristics of solid-target soft x-ray laser amplifiers by injection seeding with high harmonic pulses

Mark Berrill,[1,2,*] David Alessi,[1,2] Yong Wang,[1,2] Scott R. Domingue,[1,2] Dale H. Martz,[1,2] Brad M. Luther,[1,2] Yanwei Liu,[1,3] and Jorge J. Rocca[1,2,4]

[1]*National Science Foundation Engineering Research Center for Extreme Ultraviolet Science and Technology, Colorado State University, Fort Collins, Colorado 80523, USA*

[2]*Electrical and Computer Engineering Department, Colorado State University, Fort Collins, Colorado 80523, USA*

[3]*College of Engineering, University of California at Berkeley, Berkeley, California 94720, USA*

[4]*Physics Department, Colorado State University, Fort Collins, Colorado 80523, USA*

**Corresponding author: berrill@engr.colostate.edu*

Received February 11, 2010; revised June 10, 2010; accepted June 13, 2010; posted June 18, 2010 (Doc. ID 124159); published July 1, 2010

Injection seeding of solid-target soft x-ray laser amplifiers with high harmonic pulses is shown to dramatically improve the far-field laser beam profile and reduce the beam divergence. Measurements and two-dimensional simulations for a 13.9 nm nickel-like Ag amplifier show that the amplified beam divergence depends strongly on the seed and can therefore be controlled by selecting the divergence of the seed. The near-field beam size of both the seeded and unseeded lasers is shown to be determined by the size of the gain region and the divergence of the amplified beams.

OCIS codes: 140.7240, 340.7480.

High-average-power tabletop soft x-ray (SXR) laser beams at wavelengths between 10 and 30 nm have been generated by optical laser excitation of solid targets [1–5]. However, the beams produced by these amplifiers are characterized by relatively large beam divergence (5–15 mrad) [1–5], highly speckled patterns (Fig. 1(a) and [6]), and limited spatial [7] and temporal coherence [8]. Previous work by Tanaka *et al.* demonstrated a significantly reduced far-field divergence and increased spatial coherence using an injection technique scheme that makes use of two SXR plasma amplifiers [9]. Injection-seeding of SXR amplifiers with high harmonic (HH) pulses is a promising technique for improving the characteristics of SXR lasers that has additional advantages [10–15]. In addition to a reduced beam divergence and providing full spatial coherence [12], this technique can generate intense SXR laser pulses with full temporal coherence [14], shorter pulse width [14], and defined polarization [10]. The seeding of broad bandwidth solid-target SXR laser amplifiers with HH pulses has the potential of generating femtosecond SXR laser pulses [10,14]. Herein we report the results of the characterization of the near-field and far-field patterns of a seeded 13.9 nm solid-target amplifier that show that injection-seeding dramatically decreases the beam divergence and results in a nearly Gaussian far-field profile [Fig. 1(b)]. The far-field divergence is shown to be strongly dependent on that of the initial HH seed and can therefore be tailored by selecting the divergence of the seed. The near-field beam size of both the seeded and unseeded amplifiers is shown to depend on the size of the gain region and the beam divergence.

The experiments were conducted with a nickel-like Ag SXR laser amplifier, excited using pump conditions similar to those described in [13]. An 815 nm Ti:sapphire laser was used to create a sequence of pump pulses consisting of a 10 mJ prepulse of 120 ps duration, followed after about 5 ns by a second ~350 mJ prepulse impinging at normal incidence, which in turn was followed after 200 ps by an ~0.9 J heating pulse of 6.7 ps duration impinging at a grazing incidence angle of 23°. The pump pulses were focused onto the target to form a 30 μm × 4.1 mm FWHM long line. The length of the target was 3 mm. A small portion of the pump laser energy (~20 mJ) was split, compressed in a separate pulse compressor, and focused into an Ne gas jet with a $f = 1.2$ m lens to produce fifty-ninth seed pulses. The output of the gas jet was relay imaged onto a ~100 μm diameter spot at the input of the plasma amplifier using a gold-coated toroidal mirror designed to operate at a grazing incidence angle of 10°.

The plasma amplifier was simulated using a two-dimensional (2D) hydrodynamic plasma model developed in-house. The left column in Fig. 2 shows the evolution of the main plasma properties as a function of distance from the target, and the right column shows the

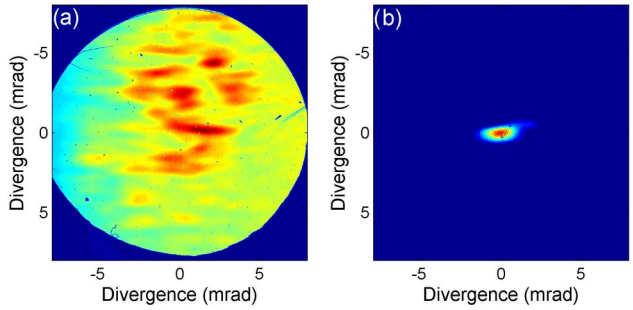

Fig. 1. (Color online) Comparison of the far field from an (a) unseeded 13.9 nm Ni-like Ag amplifier and of (b) the same amplifier seeded by HH pulses. Injection seeding results in an ~10× decrease of the beam divergence. The circular aperture in (a) is from a filter frame.

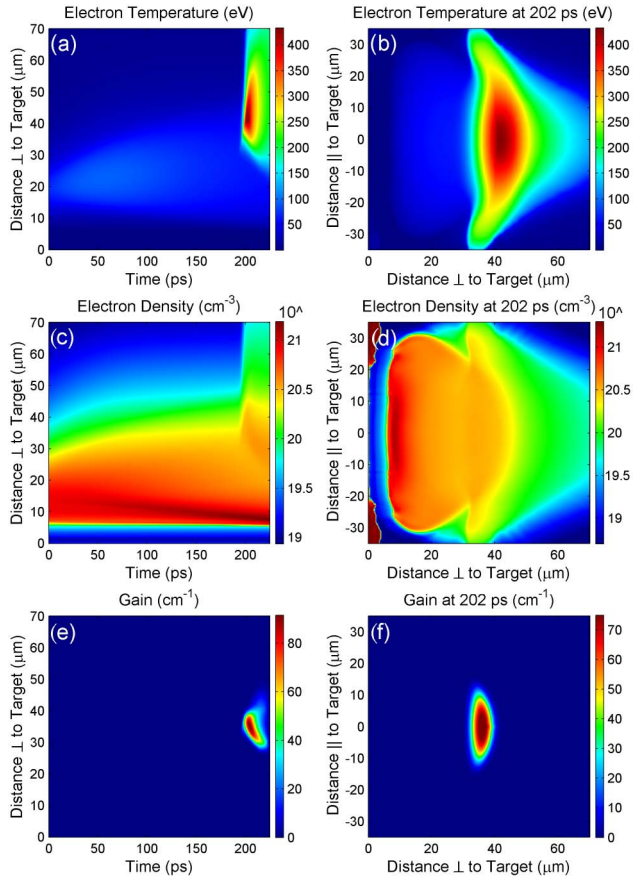

Fig. 2. (Color online) Simulated plasma characteristics and gain distribution of a 13.9 nm SXR laser plasma amplifier. The excitation conditions are those described in the text.

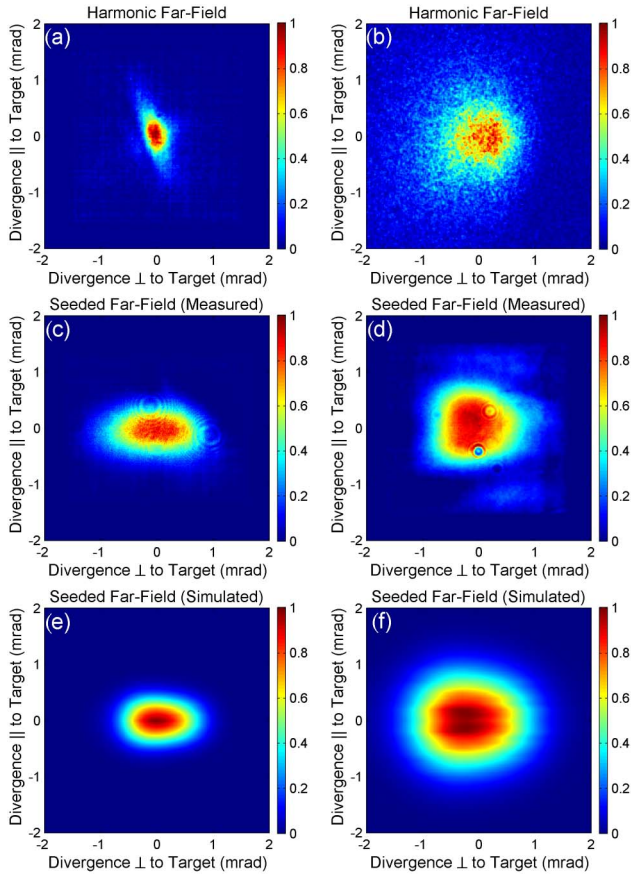

Fig. 3. (Color online) Comparison of far-field profiles of (a) and (b) measured HH seeds with two different divergences; (c), (d) corresponding measured seeded laser beams; and (e), (f) simulated seeded laser beams.

2D spatial distribution of the electron density, electron temperature, and small-signal gain at the time delay of 202 ps after the peak of the main prepulse. The prepulse is computed to heat the plasma to ~90 eV, resulting in a degree of ionization of ~18 at the time of arrival of the short pulse. The short pulse rapidly heats the plasma to ~400 eV in the region where the electron density is $2–3 \times 10^{20}$ cm^{-3}, resulting in a small-signal gain coefficient of ~80 cm^{-1} at 35 μm from the target surface. These results were then fed into a 3D ray-trace postprocessor code that can compute beam profiles for direct comparison with the experiments. This code fully treats saturation effects by solving the atomic rate equations with stimulated emission at each point along the SXR amplifier.

The far-field beam pattern was recorded by placing a back-thinned CCD detector at 0.86 m from the plasma. Two 0.3-μm-thick Zr filters with Parylene support were used to filter visible light and attenuate the SXR lasers. Laser experiments were conducted using two different seed pulse divergences to study the dependence of the amplified beam on the seed. A comparison with the simulated far-field beam profiles for the two cases is illustrated in Fig. 3 along with the corresponding profile of the HH seed. When a HH seed pulse with an FWHM divergence of $0.5 \pm 0.03 \times 0.7 \pm 0.04$ mrad in the directions perpendicular and parallel to the target, respectively, was used to seed the plasma, an amplified pulse with a divergence of $1.4 \pm 0.14 \times 0.7 \pm 0.07$ mrad was measured as a result [Fig. 3(c)]. Simulations agree in showing that the divergence of the amplified beam in the direction parallel to the target surface closely resembles that of the seed beam, while the divergence perpendicular to the target surface is larger due to refraction. When the divergence of the HH seed was increased to $1.6 \pm 0.3 \times 1.4 \pm 0.4$ mrad, an amplified pulse with a divergence of $1.5 \pm 0.08 \times 1.2 \pm 0.15$ mrad was measured [Fig. 3(d)]. The results show that when the divergence of the input HH seed is larger than ~1 mrad the far field of the amplified seed is almost completely dominated by the seed, while for smaller divergences it is controlled by both the input seed and refraction. These beam divergences are nearly 1 order of magnitude smaller than those corresponding to the unseeded amplifier (Fig. 1).

The near-field beam pattern was recorded by projecting the exit plane of the amplifier onto the CCD with 15.2× magnification using the combination of a concave ($R = 0.5$ m) mirror and a flat Mo-Si multilayer mirror placed on a Z-fold configuration. A pinhole was placed in front of the imaging mirror to help discriminate the seeded beam from the amplified spontaneous emission (ASE). Figure 4 compares the measured near-field profiles of the unseeded and seeded beams. The location of the center of the near-field beam spot with respect to the target surface [Figs. 4(a) and 4(c)] is dominantly determined by the position of the peak of the gain [~35 μm from the target in Fig. 2(f)] and was measured

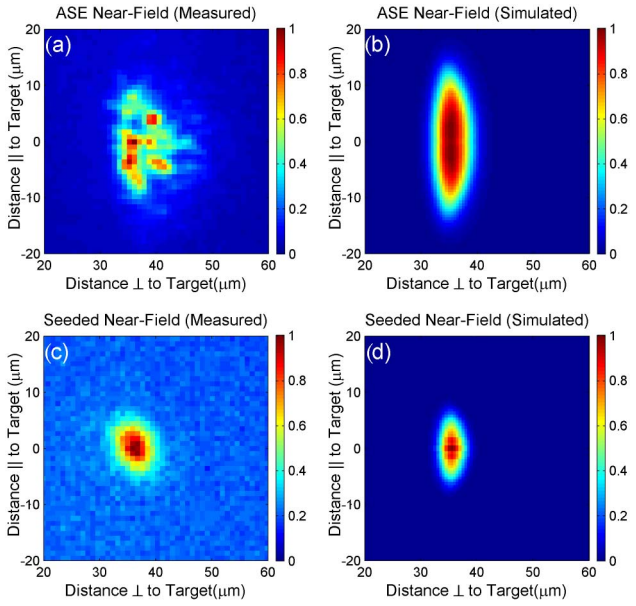

Fig. 4. (Color online) Measured and simulated near-field beam profiles for the ASE and seeded lasers.

to be at a distance of 33 ± 4 μm, in good agreement with the simulated near-field profile [Figs. 4(b) and 4(d)]. Model simulations show that the location of the gain is, in turn, dependent on the early prepulse that is responsible for creating the initial plasma profile and that the absence of this prepulse shifts the gain closer to the target surface (to a distance of ~15 μm). As the seed propagates through the plasma amplifier, its intensity quickly saturates, yielding a near-field profile that is dominantly determined by the spatial distribution of the saturation fluence integrated over the amplifier length. The measured near-field size of the unseeded ASE laser [Fig. 4(a)] is characterized by an FWHM of $11.3 \pm 4 \times 13.3 \pm 3$ μm in the directions perpendicular and parallel to the target surface, respectively. The measured size of the seeded laser beam [Fig. 4(c)] is smaller, $6.0 \pm 0.6 \times 8.3 \pm 1.5$ μm. The larger near-field spot size of the ASE laser in the direction parallel to the target surface is due to the larger divergence of the ASE laser, which allows rays with different trajectories to amplify across the entire gain region. By contrast, the narrow divergence of the HH seed causes all the rays to effectively take similar paths, resulting in a narrower beam profile. This size difference is enhanced in the direction parallel to the target surface due to the larger gain size and to the fact that the seeded beam is more sensitive to refraction caused by the electron density profile of the plasma amplifier [Fig. 2(d)], which acts as a weak negative lens. It should be noticed that the simulation results shown in Fig. 4 assume a perfect overlap between the laser pulses. Computations show that a 10 μm misalignment causes the gain region and resulting near-field beam size to decrease by ~20% in the direction parallel to the target surface.

In conclusion, we have characterized for the first time (to our knowledge) the near-field and far-field distributions of an injection-seeded solid-target SXR laser amplifier with experiments and 2D simulations. Seeding is shown to reduce the far-field divergence by 1 order of magnitude and to allow for control of the far-field beam characteristics by tailoring the divergence of the seed.

This work was supported by the National Science Foundation (NSF) Center for Extreme Ultraviolet Science and Technology under NSF award EEC-0310717 and by the Chemical Sciences, Geosciences and Biosciences Division, Office of Basic Energy Sciences, Office of Science, United States Department of Energy (DOE), using a facility initially made possible with the support of the W. M. Keck Foundation. M. B. acknowledges support from the DOE Computational Science Graduate Fellowship program under grant DE-FG02-97ER25308.

References

1. Y. Wang, M. A. Larotonda, B. M. Luther, D. Alessi, M. Berrill, V. N. Shlyaptsev, and J. J. Rocca, Phys. Rev. A **72**, 053807 (2005).
2. J. J. Rocca, Y. Wang, M. A. Larotonda, B. M. Luther, M. Berrill, and D. Alessi, Opt. Lett. **30**, 2581 (2005).
3. H. T. Kim, I. W. Choi, N. Hafz, J. H. Sung, T. J. Yu, K.-H. Hong, T. M. Jeong, Y. C. Noh, D. K. Ko, K. A. Janulewicz, J. Tümmler, P. V. Nickles, W. Sandner, and J. Lee, Phys. Rev. A **77**, 023807 (2008).
4. D. Zimmer, B. Zielbauer, M. Pittman, O. Guilbaud, J. Habib, S. Kazamias, D. Ros, V. Bagnoud, and T. Kuehl, Opt. Lett. **35**, 450 (2010).
5. D. Alessi, D. H. Martz, Y. Wang, M. Berrill, B. M. Luther, and J. J. Rocca, Opt. Lett. **35**, 414 (2010).
6. A. Klisnick, O. Guilbaud, D. Ros, K. Cassou, S. Kazamias, G. Jamelot, J. C. Lagron, D. Joyeux, D. Phalippou, Y. Lechantre, M. Edwards, P. Mistry, and G. J. Tallents, J. Quant. Spectr. Rad. Trans. **99**, 370 (2006).
7. Y. Liu, Y. Wang, M. A. Larotonda, B. M. Luther, J. J. Rocca, and D. T. Attwood, Opt. Express **14**, 12872 (2006).
8. R. Smith, J. Dunn, J. Hunter, J. Nilsen, S. Hubert, S. Jacquemot, C. Remond, R. Marmoret, M. Fajardo, P. Zeitoun, L. Vanbostal, C. Lewis, M. Ravet, and F. Delmotte, Opt. Lett. **28**, 2261 (2003).
9. M. Tanaka, M. Nishikino, T. Kawachi, N. Hasegawa, M. Kado, M. Kishimoto, K. Nagashima, and Y. Kato, Opt. Lett. **28**, 1680 (2003).
10. P. Zeitoun, G. Faivre, S. Sebban, T. Mocek, A. Hallou, M. Fajardo, D. Aubert, P. Balcou, F. Burgy, D. Douillet, S. Kazamias, G. de Lachèze-Murel, T. Lefrou, S. le Pape, P. Mercère, H. Merdji, A. S. Morlens, J. P. Rousseau, and C. Valentin, Nature **431**, 426 (2004).
11. T. Mocek, S. Sebban, G. Maynard, P. Zeitoun, G. Faivre, A. Hallou, M. Fajardo, S. Kazamias, B. Cros, D. Aubert, G. de Lachèze-Murel, J. P. Rousseau, and J. Dubau, Phys. Rev. Lett. **95**, 173902 (2005).
12. Y. Wang, E. Granados, M. A. Larotonda, M. Berrill, B. M. Luther, D. Patel, C. S. Menoni, and J. J. Rocca, Phys. Rev. Lett. **97**, 123901 (2006).
13. Y. Wang, E. Granados, F. Pedaci, D. Alessi, B. M. Luther, M. Berrill, and J. J. Rocca, Nat. Photonics **2**, 94 (2008).
14. Y. Wang, M. Berrill, F. Pedaci, M. M. Shakya, S. Gilbertson, Z. Chang, E. Granados, B. M. Luther, M. A. Larotonda, and J. J. Rocca, Phys. Rev. A **79**, 023810 (2009).
15. F. Pedaci, Y. Wang, M. Berrill, B. Luther, E. Granados, and J. J. Rocca, Opt. Lett. **33**, 491 (2008).